ν_μ Disappearance in MicroBooNE using the Deep Learning $1\mu1p$ Selection

MICROBOONE-NOTE-1106-PUB

The MicroBooNE Collaboration
MicroBooNE_Info@fnal.gov

May 29, 2022

Abstract:

We test a 3+1 model with the MicroBooNE data using a $1\mu1p$ selection developed using Deep-Learning-based reconstruction. In order to test this model we apply a muon neutrino disappearance effect to the selection, and search across a grid of oscillation model parameters using a Feldman Cousins technique. We determine MicroBooNE's sensitivity across this model parameter space, and perform several validation studies to test this study's robustness. Finally, we examine the allowed and excluded regions per MicroBooNE's data at 90% confidence, using a data set corresponding to 6.67×10^{20} protons on target. The null model remains allowed, and several of the high-disappearance models are excluded.

Contents

1 Introduction

Under the short-baseline assumption, the survival probability for muon neutrinos in a 3+1 sterile neutrino model is

$$P_{\nu_\mu \to \nu_\mu} = 1 - \sin^2 2\theta_{\mu\mu} \sin^2(1.27\Delta m^2_{41} L/E). \quad (1)$$

Where Δm^2_{41} is the mass splitting associated with the additional mass state, and $\sin^2 2\theta_{\mu\mu}$ is the term associated with the extension to the PMNS matrix under the 3+1 model. L is the length of the baseline the neutrino has traveled in km, and E its energy in GeV. This formula dictates the effects of muon neutrino disappearance, whereby muon neutrinos oscillate through their connection to ν_4 to some other flavor state. In particular this modeling follows the "short baseline approximation" where $\Delta m^2_{21} \approx \Delta m^2_{32} \approx 0$ when considering the new mass states' splitting from the standard model neutrinos Δm^2_{41}, as described in [1]. When used to model our expected spectrum of neutrino interactions based on simulated data, both L and E are the true values for a given simulated neutrino event.

A 3+1 sterile neutrino model can be used to explain the ν_e-like low-energy excess (LEE) observed in MiniBooNE [2] and LSND [3] via ν_e appearance phenomena [1]. This phenomenology can be explained as muon neutrinos disappearing via oscillations then yielding proportionally more ν_e. However, presently, muon neutrino disappearance via a 3+1 model search has not been observed.

Within this note we search for muon neutrino disappearance in the MicroBooNE Liquid Argon Time Projection Chamber (LArTPC) [4] using a selection of $1\mu1p$ events produced using a Deep Learning reconstruction for MicroBooNE's first LEE search [5]. The reconstruction and selection of these events is the first to utilize calorimetric energy reconstruction via direct measurement of both the proton and muon, and the kinematics surrounding the neutrino interaction in order to perform a sterile-neutrino-based disappearance oscillation measurement. The resulting energy resolutions are $2.5 \pm 0.1\%$ for protons and $3.4 \pm 0.1\%$ for muons [6]. In both cases the energies are calculated based on the length of the reconstructed track length according to the stopping power of protons and muons. We note that this analysis builds up from the work demonstrated in [7]. This analysis uses the $1\mu1p$ event selection described in [5], and the event simulation includes sophisticated modeling of meson exchange current (MEC) interactions and other nuclear effects [5, 8]. This $1\mu1p$ selection is expected to be $\sim$ 98% pure in muon neutrino interactions, of which $\sim$ 75.2% are well-reconstructed charged-current quasi-elastic ν_μ interactions. This selection is shown in Figure 1. The remaining $\sim$ 2% of events are primarily misreconstructed cosmic ray muon interactions, with only ~ 2 ν_e events out of $\sim$ 4480 total events predicted in a data set containing 6.67×10^{20} POT. As such, most of the spectrum is free to disappear. Using this selection and Equation 1 we can oscillate the expectation across a variety of model parameters to acquire the expectation under various 3+1 models.

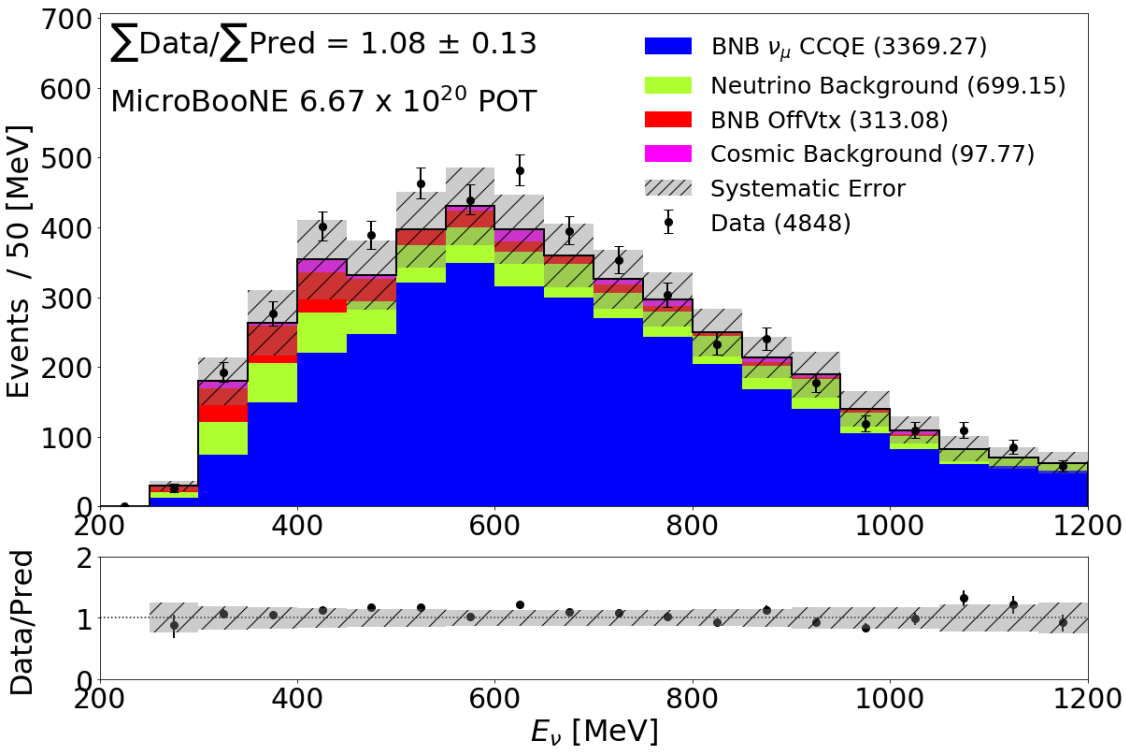

Figure 1: Stacked histogram of expectation binned in reconstructed ν_μ energy after final selection and overlaid with data from Runs 1-3, corresponding to 6.67×10^{20} POT [5].

2 Disappearance Search Window

Throughout this ν_μ disappearance search we will test the consistency of many different 3+1 sterile neutrino models with MicroBooNE data. We perform a 25×25 grid search over the two parameters $\sin^2 2\theta_{\mu\mu}$ and Δm^2_{41}, with points logarithmically spaced with $\sin^2 2\theta_{\mu\mu} \in [0.01, 1]$ and $\Delta m^2_{41} \in [0.01, 100]$ eV^2. Table 1 shows the 25 bin center values of $\sin^2 2\theta_{\mu\mu}$ and Δm^2_{41} used in this grid search.

The $\sin^2 2\theta_{\mu\mu}$ term in the disappearance formula controls the amplitude of the effect, while the Δm^2_{41} eV^2 parameter effects the frequency of the oscillation. Figure 2 shows a cartoon of this disappearance effect. The black curve shows the original expectation, the red curve shows the portion of events that disappear, or $P_{\mu\to\mu}$ multiplied by the original flux, and the blue curve shows the modified spectrum after disappearance beneath the original spectrum. Note that the flux shown is not the Fermilab Booster Neutrino Beam (BNB) flux seen at MicroBooNE and is instead designed for illustrative purposes.

Similarly, Figure 3 shows the same cartoon, with the only difference being that the bin width is set to 50 MeV, this analysis' histogram bin width. This width was chosen based on the energy resolution demonstrated in [5]. Therefore this version of the cartoon demonstrates the change in coarseness of the disappearance effect placed on the spectrum.

We create the "maximally disappeared" spectrum for each of these 25 values of Δm^2_{41} eV^2, by setting $\sin^2 2\theta_{\mu\mu}$ to the greatest bin value searched in this analysis, 0.912, to see the greatest change possible within our search. These 25 spectra in blue, plotted against the null

Bin Index	Δm^2_{41} eV^2	$\sin^2 2\theta_{\mu\mu}$
1	0.012	0.011
2	0.017	0.013
3	0.025	0.016
4	0.036	0.019
5	0.052	0.023
6	0.076	0.028
7	0.110	0.033
8	0.158	0.040
9	0.229	0.048
10	0.331	0.058
11	0.479	0.069
12	0.692	0.083
13	1.000	0.100
14	1.445	0.120
15	2.089	0.145
16	3.020	0.174
17	4.365	0.209
18	6.310	0.251
19	9.120	0.302
20	13.183	0.363
21	19.055	0.437
22	27.542	0.525
23	39.811	0.631
24	57.544	0.759
25	83.176	0.912

Table 1: Bin centers for the two parameters in the fit Δm^2_{41} eV^2 and $\sin^2 2\theta_{\mu\mu}$.

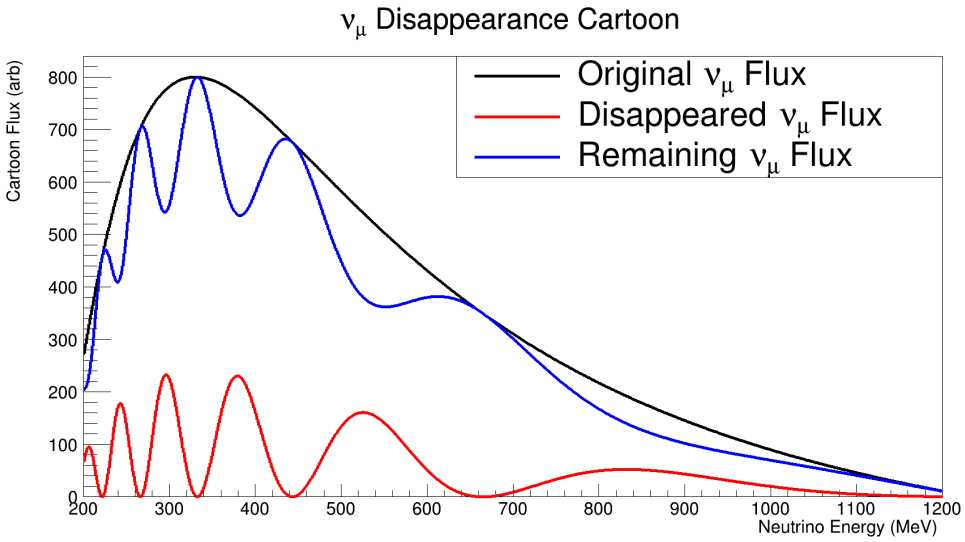

Figure 2: A cartoon of the method by which one builds a ν_μ disappearance spectrum from an initial prediction under the 3ν hypothesis. Note the flux shown is a cartoon, and not the BNB flux.

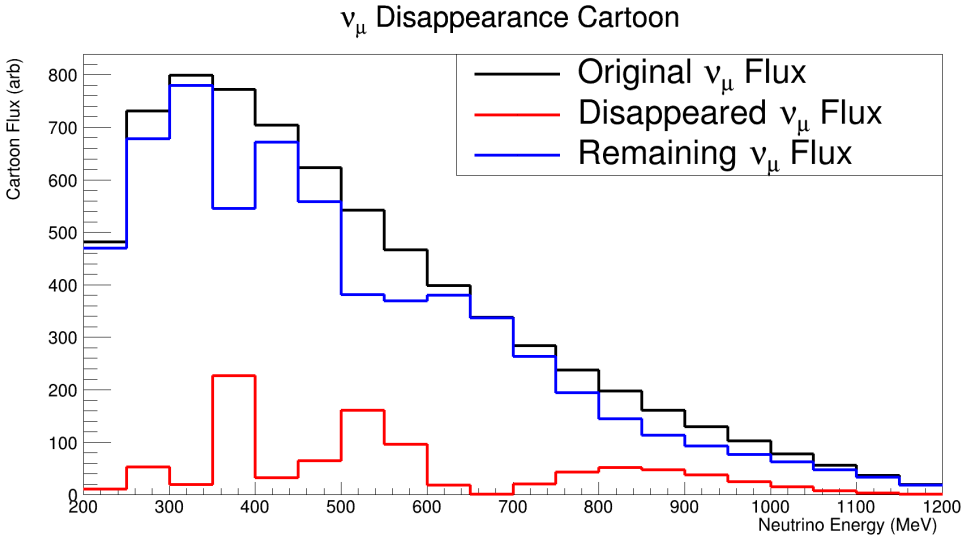

Figure 3: Another cartoon of ν_μ disappearance, however now using 50-MeV-wide bins as will be used in the data analysis. Note the flux shown is a cartoon, and not the BNB flux.

oscillation spectrum in black, are shown in Figure 4.

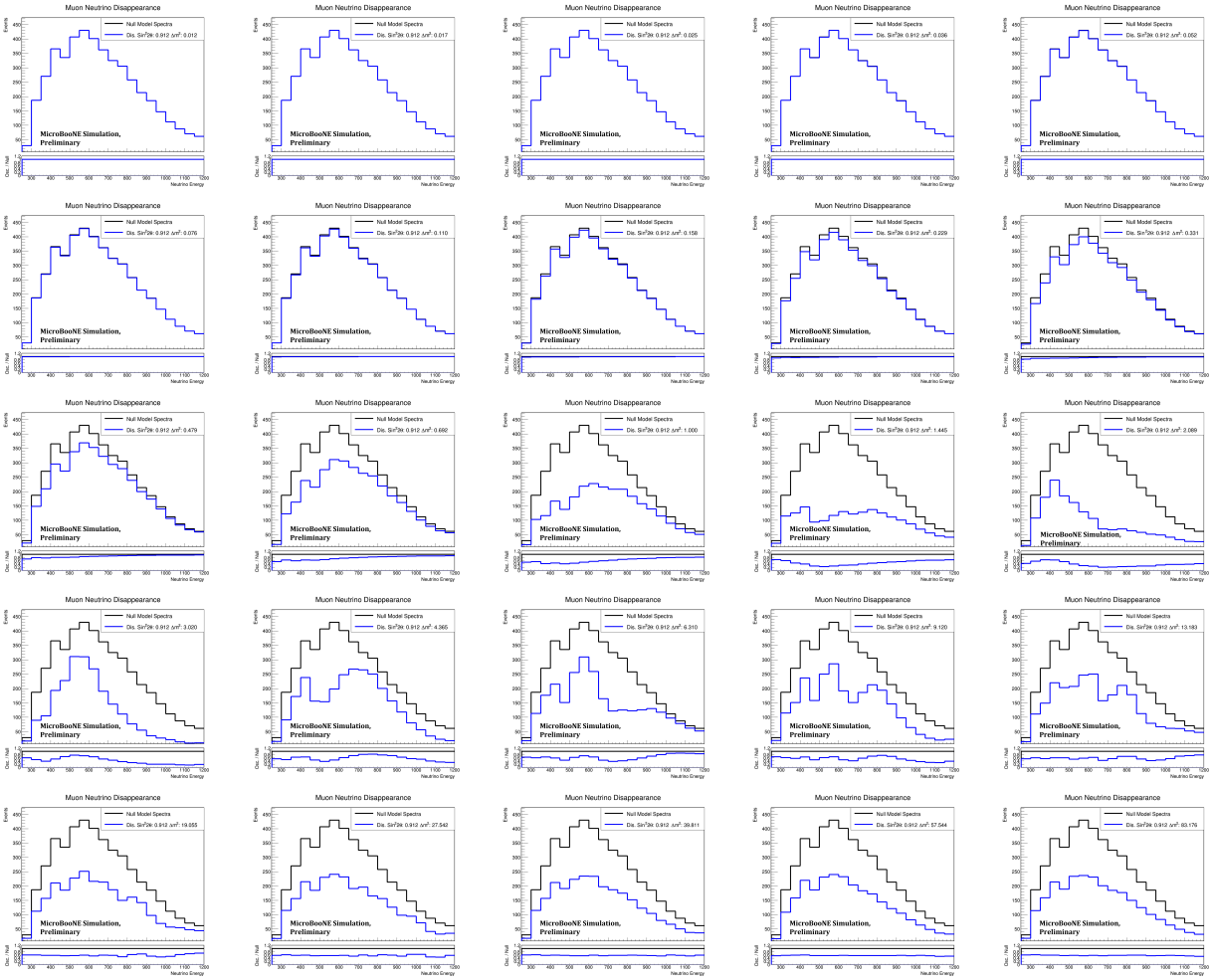

Figure 4: For all 25 values of Δm^2_{41}, the predicted spectrum after disappearance is shown against the null model spectrum. As $\sin^2 2\theta_{\mu\mu}$ is an amplitude, the maximum grid value is used for each plot to maximize the disappearance effect.

3 Negative Log Likelihood Ratio as a Test Statistic

This analysis' test statistic is defined as the negative log likelihood ratio, termed R, defined as

$$R \equiv -2ln(L_{PT}/L_{bf}) = \chi^2_{PT} + ln(|2\pi M_{PT}|) - \chi^2_{bf} - ln(|2\pi M_{bf}|). \tag{2}$$

Here PT refers to the grid point in the 25×25 grid we are testing and bf refers to the best fit (minimum) negative-log-likelihood when comparing an observation to all the grid points. M is the covariance matrix encapsulating the uncertainties associated with the selection, as described below, and χ^2 is defined as

$$\chi^2(\Theta) = \sum_{ij}^{bins} (N_i^{obs} - N_i^{pred}(\Theta)) M_{ij}^{-1} (N_j^{obs} - N_j^{pred}(\Theta)), \tag{3}$$

where Θ refers to the disappearance model being examined, and N refers to the number of events in a given bin for the prediction or observation depending on superscript.

4 Analysis Uncertainty

The total fractional covariance matrix from the systematic uncertainties is shown in Figure 5, reproduced from [5]. This fractional matrix gets scaled to the different expectations when appropriate, whether they are the null model expectation or some disappeared spectrum. As such, smaller applied expectations receive smaller absolute uncertainties. We also examine the uncorrelated fractional uncertainty broken down by type across the analysis energy range, in Figure 6. Explanations of these different sources of uncertainty are provided in [5].

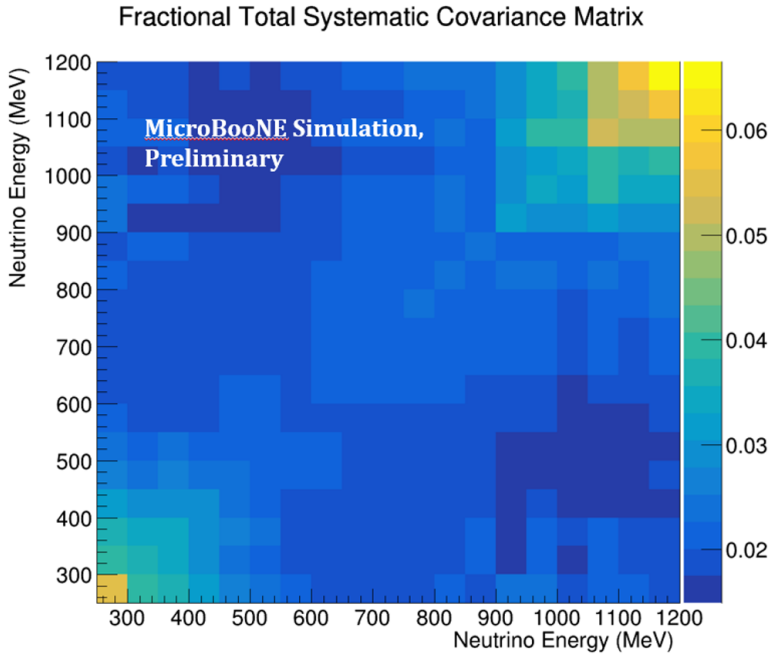

Figure 5: The total, fractional systematic covariance matrix for the $1\mu1p$ analysis.

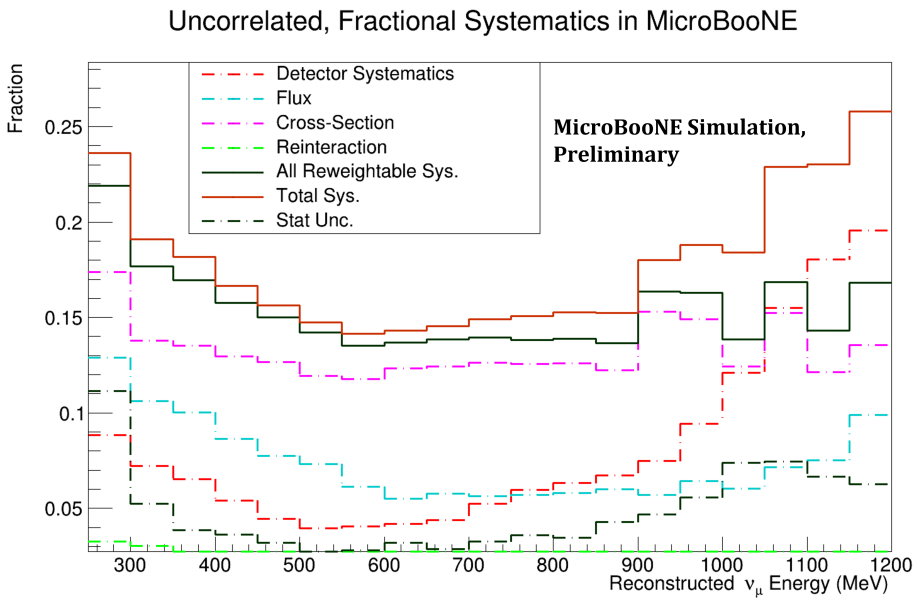

Figure 6: The uncorrelated fractional systematics broken down by type. The statistical uncertainty associated with the expectation samples is also shown for comparison.

5 Determining a Sensitivity

We calculate the test statistic, R for every point in grid space. We can determine this analysis' sensitivity to a parameter exclusion region by setting the 'observation' to exactly the null expectation. The array of test R values is shown in Figure 7, both in linear and logarithmic z-axis scale. Higher values of R indicate a greater disparity between the observation from this grid point's expectation compared to the observation's best fitting model. Note that the null model is effectively at the bottom-left of the these style plots, with both oscillation parameters effectively 0. We note that this estimator, the negative-log-likelihood-ratio, has a bias towards preferring spectra with fewer events. This comes about from the determinant term in the calculation which favors lower spectra, and results in a best fit different than the null expectation when inputting the null as observation. However, the bias toward a smaller spectrum cannot be too high, or else it will be offset by the χ^2 terms in the test statistic. In this sensitivity test, the best fit ends up in a region of models that all appear similar to the null expectation, and separate from the high-disappearance region which the analysis expects to be able to exclude.

The R values in this plot demonstrate how different the null observation is from a point's expectation compared to its best fit expectation. Note that much of the search is a region of low R values, where the null observation is not very different from the expectation. Within this degeneracy of models we expect little discrimination power. Instead, we expect greater power in the high R value region.

We use a Feldman Cousins-based frequentist analysis to determine the critical values to which these test R values can be compared to in order to determine the sensitivity region. We throw 1000 "universes" using the covariance matrix at each point of parameter space. Each universe is treated as an observation, then its R value is calculated. The critical threshold,

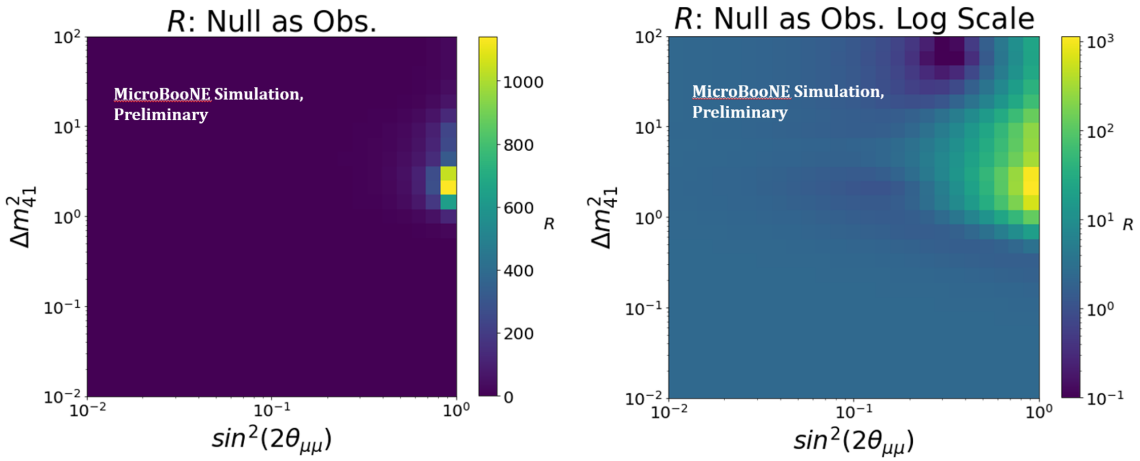

Figure 7: The test R values across every point in the parameter space. The left plot displays the raw R value, while the right shows the same values at log scale.

R_C, is the value below which 90% of calculated R values in the 1000 universe distribution fall. This process is depicted in Figure 8. Instead of using the Feldman Cousins method, one could use Wilks' theorem to assume that R follows a χ^2 distribution with 2 degrees of freedom. The Feldman Cousins calculated R_C values are shown in Figure 9, which also shows a comparison to the Wilks' 2 degree of freedom threshold of 4.6. This comparison plot shows the fractional difference to the 4.6 threshold, and where it is non-zero the Feldman Cousins and Wilks' values differ.

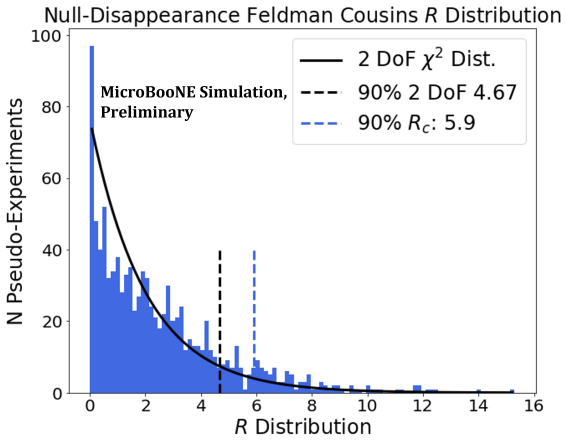

Figure 8: The distribution of R across 1000 pseudo-experiments for the null, no-disappearance, hypothesis as Θ_T, shown in blue. The plot also contains the expected χ^2 distribution for two degrees of freedom. Vertical lines are drawn for the 90% CL of each distribution, such that 90% of the distribution is to the left of the vertical line.

This resulting sensitivity contour borders the region where the test R values are greater than the R_C values. This is shown in Figure 10. MiniBooNE's sensitivity is also shown [9]. We also produce two additional sensitivities: one assuming MicroBooNE had no systematic uncertainty (Figure 11) and another assuming MicroBooNE had 40× the present data statistics (Figure 12). This factor of 40 was chosen because it represents the difference in number

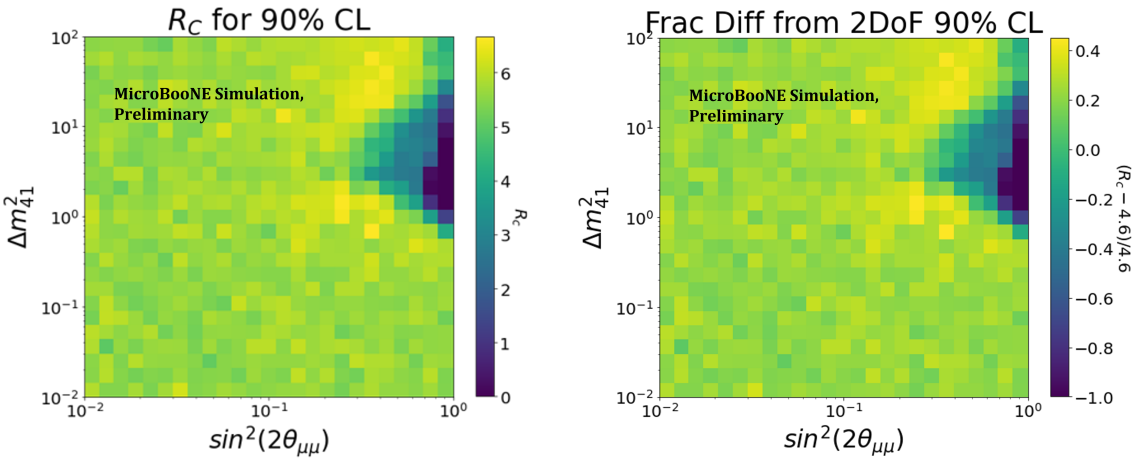

Figure 9: The critical R values for 90% CL across every point in this parameter space. The left plot displays the raw R_C value, while the right shows the fractional difference in R_C from a 2-degree-of-freedom scenario.

of events used in the MiniBooNE analysis compared to this analysis. These demonstrate that while the analysis could be improved by adding more statistics, or reducing systematic uncertainty, it is more limited by the systematic uncertainty. Lastly, a sensitivity is also calculated as though this analysis only had one energy bin, thereby acting as a 'rate-only' study, where oscillation shape information is invisible. This is shown in Figure 13. This final sensitivity uses an R_C of 4.6, via Wilks' theorem, which expects the R distribution to follow a χ^2 distribution, rather than recompute the R_C via Feldman Cousins method for a 1-bin analysis.

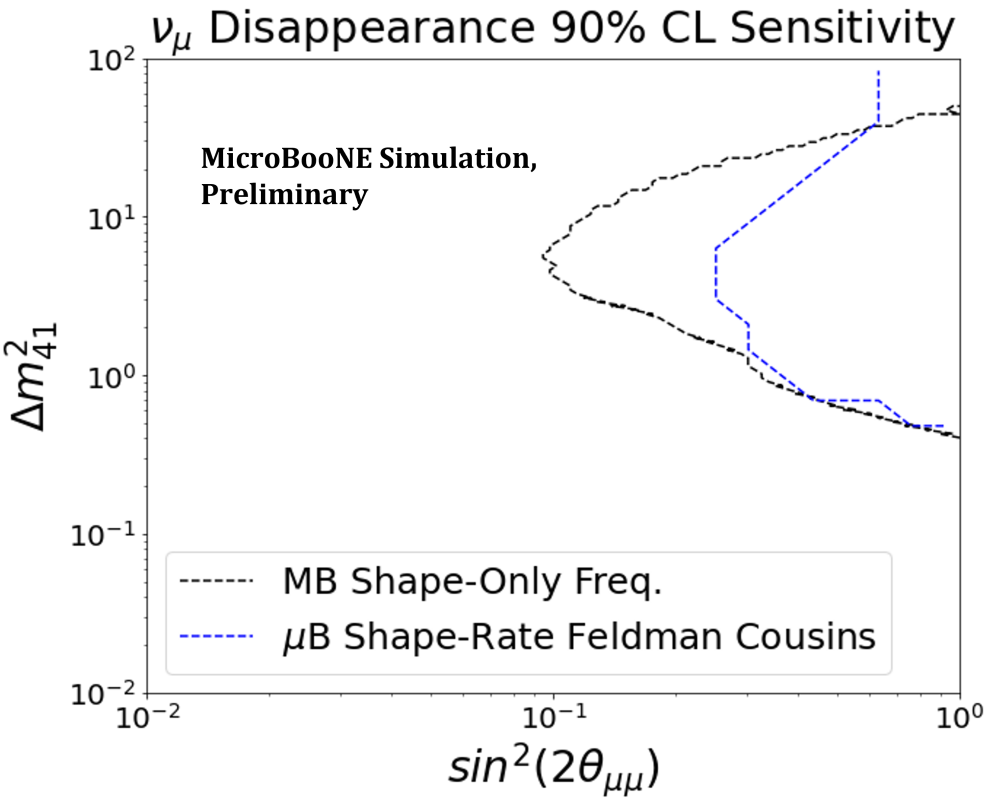

Figure 10: MicroBooNE's 90% sensitivity contour for the parameter-space scan is shown, using the Feldman Cousins method of determining R_C. MiniBooNE's ν_μ disappearance sensitivity is overlaid [9].

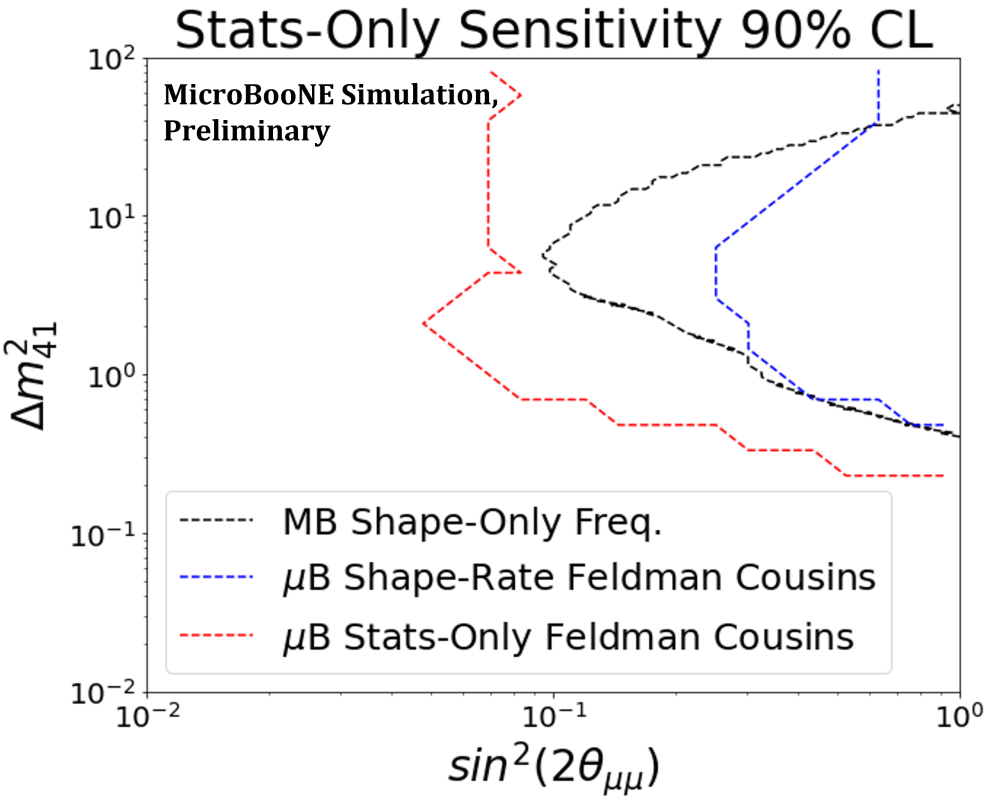

Figure 11: For the stats-only regime, MicroBooNE's 90% sensitivity contour for the parameter-space scan is shown, using the Feldman Cousins method of determining R_C. Both the MicroBooNE full sensitivity, and MiniBooNE's ν_μ disappearance sensitivity are overlaid [9], both of which include full evaluation of systematic uncertainties.

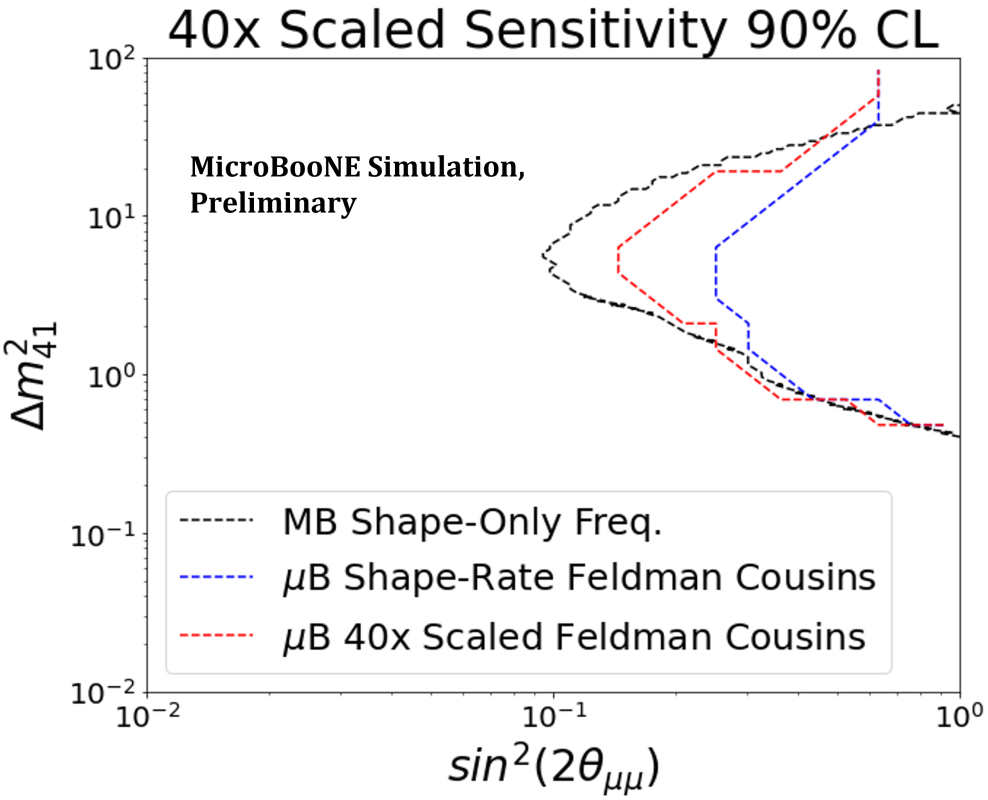

Figure 12: For the 40x scaled regime, MicroBooNE's 90% sensitivity contour for the parameter-space scan is shown, using the Feldman Cousins method of determining R_C. Both the full MicroBooNE sensitivity for 6.67×10^{20} POT and MiniBooNE's ν_μ disappearance sensitivity are overlaid [9].

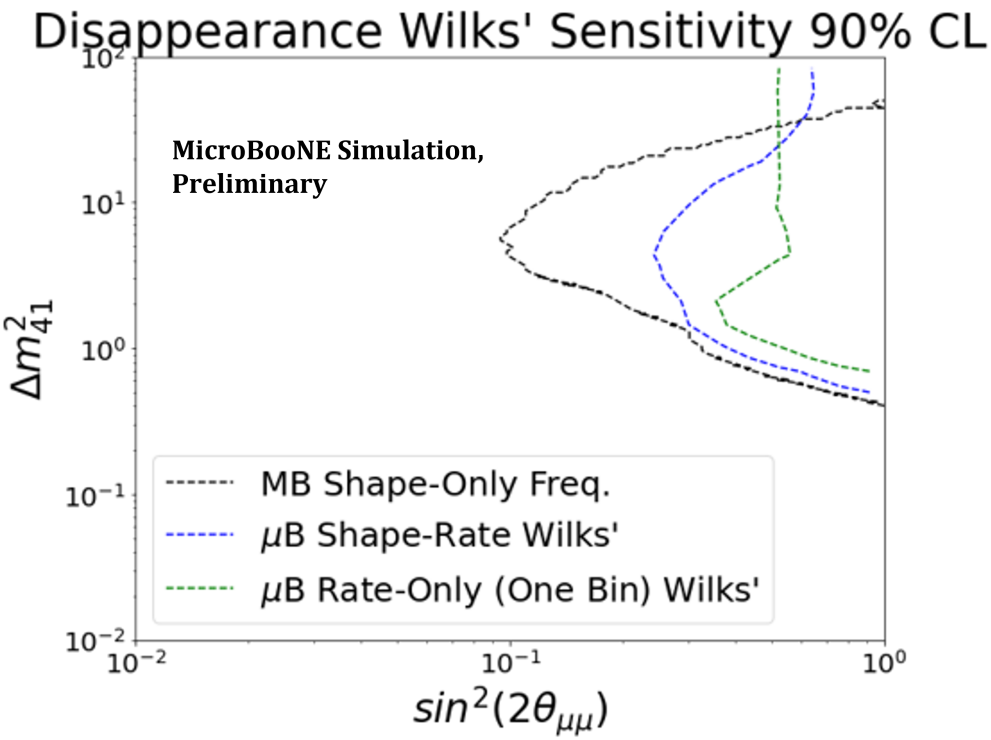

Figure 13: For the 1-bin, rate-only analysis MicroBooNE's 90% sensitivity contour for the parameter-space scan is shown, using Wilks' method of determining $R_C = 4.6$ (2 degrees of freedom). Both this standard Wilks' sensitivity and MiniBooNE's ν_μ disappearance frequentist sensitivity are overlaid [9].

6 Results: Muon Neutrino Disappearance Search using MicroBooNE Data

In this final section we perform the disappearance search using the first three years of MicroBooNE data, corresponding to 6.67×10^{20} protons on target. We now treat this observation as the data shown in Figure 1. Now the grid of R_{data} values is shown in Figure 14. While the best fit model is that of grid point $\sin^2(\theta_{\mu\mu}) = 0.12$ and $\Delta m^2_{41} = 3.02$ eV^2, this point exists within a wide region of models where we cannot discriminate the expectation from the null model. Recall that the test statistic used in this analysis has a slight bias towards spectra with fewer events (i.e. more disappearance). Figure 15 compares the best fit spectrum in red to the null expectation in blue with uncertainty bands. The data is also plotted in black.

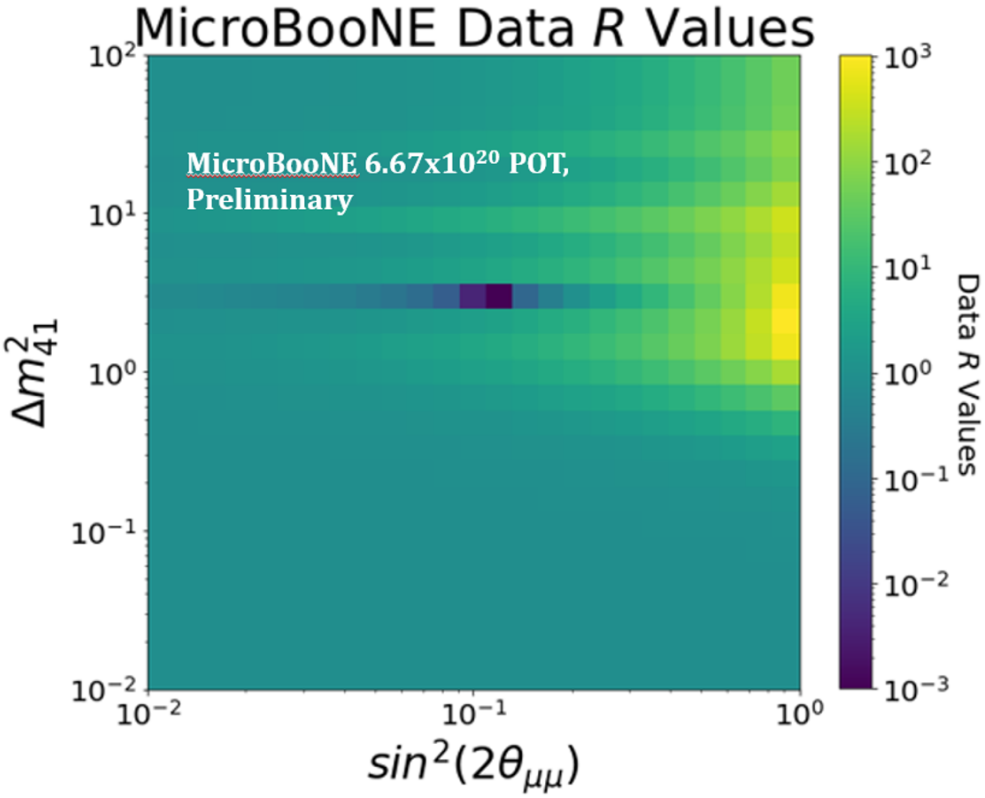

Figure 14: This grid of R_{data} values, where we input the data as the observation.

We can look at the breakdown of this calculation of R in table 2. We see there that the best fit model has a slightly lower $\ln(|2\pi M|)$ term than the null model, and the model has a slightly lower χ^2 term. However, the difference in $\ln(|2\pi M|)$ slightly outweighs that of the χ^2 term.

Finally, in Figure 16 we show the allowed (green) and excluded (white) regions of the model parameter phase space from this shape and rate, Feldman Cousins frequentist analysis. We overlay the MiniBooNE analysis' shape-only frequentist excluded region in red, which generally extends further than this analysis' exclusion curve. This analysis' sensitivity curve is also overlaid in blue. This exclusion area in white extends a bit past the sensitivity band. This is likely due to the fact that the observed data spectrum is in excess compared to the

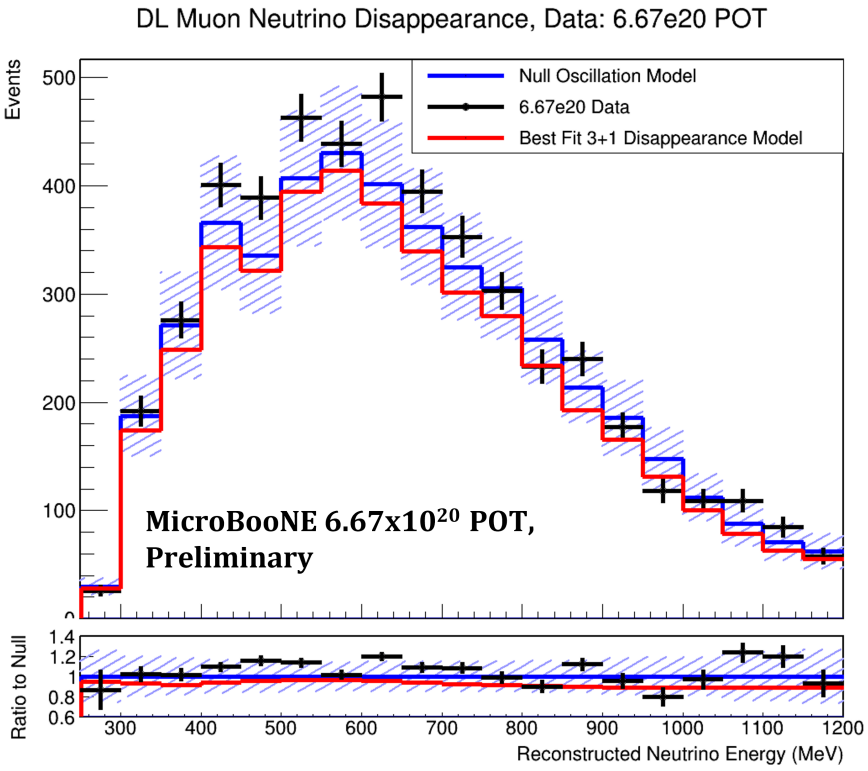

Figure 15: The different spectra of selected neutrinos. In blue the Null model expectation, with the uncertainty band surrounding it, in black the data, and in red the best fitting 3+1 sterile neutrino model.

expectation, as shown in Figure 15, which makes it easier to discriminate the observation from the heavier disappearance expectations. Specifically, because the disappeared expectation can only go down, having an observation greater than the null allows us to exclude a larger amount of phase space by putting more distance between the observation and various disappeared expectations. The null model is in agreement with MicroBooNE's data, and is still allowed. Our analysis' agreement with the null model has a p-value of 0.291.

	Null Oscillation Model	Best Fit Model	Difference
$\ln(\lvert 2\pi M \rvert)$	153.58	151.59	1.99
χ^2	21.10	22.22	-1.12
Total	174.68	173.81	0.87

Table 2: The breakdown of components of the test statistic R for the best fit point and the null oscillation model.

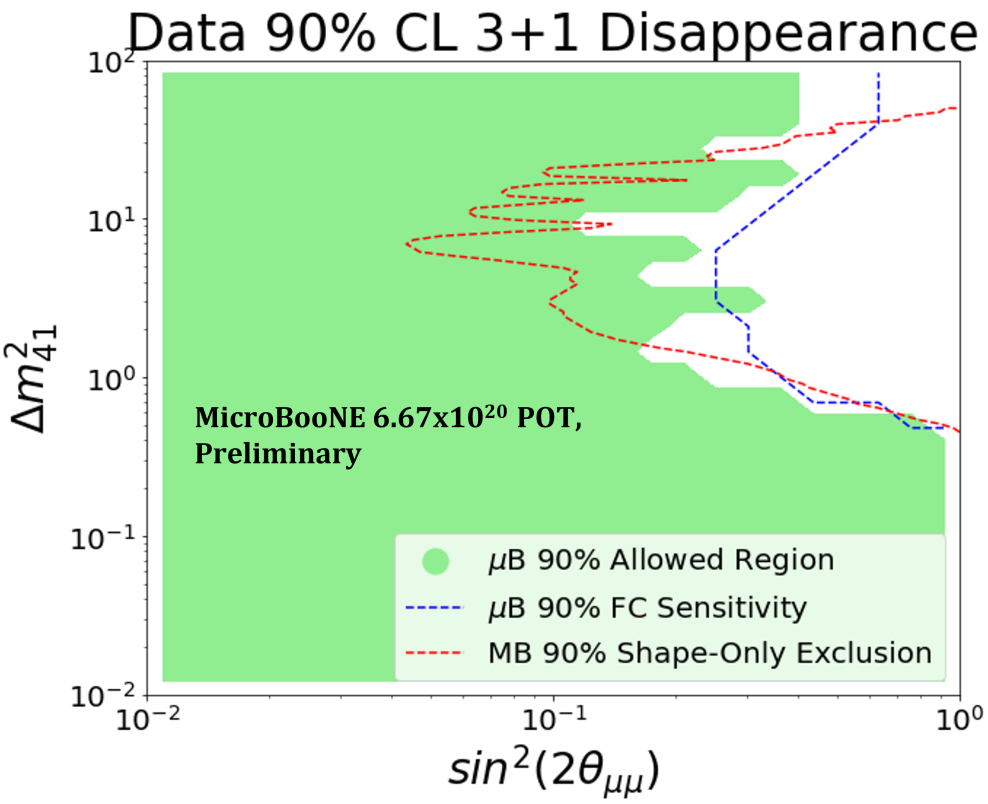

Figure 16: Using 6.67×10^{20} POT worth of MicroBooNE data we show the allowed regions of 3+1 model phase space in green, and the excluded region in white in the upper right of the plot, with sensitivity overlaid in blue. The MiniBooNE shape-only analysis' excluded curve is also overlaid in red [9].

7 Conclusions

We present a muon neutrino disappearance search using 6.67×10^{20} POT worth of data in the MicroBooNE detector. MicroBooNE's observation is consistent with ν_μ disappearance results from other experiments, and adds the power of the MicroBooNE experiment to the search for a potential 3+1 sterile neutrino model. In particular this analysis benefits from the strong energy reconstruction of both the outgoing proton and muon in this $1\mu1p$ interaction, via the calorimetric power of the MicroBooNE Liquid Argon Time Projection Chamber. We demonstrate this new robust detector technology can be used in a sterile-based oscillation study.

References

[1] A. Diaz, *et al.*, *Where are we with light sterile neutrinos*, Physics Reports vol. **884**, (2020) 1-59, [arXiv:1906.00045]

[2] A. A. Aguilar-Arevalo, *et al.* (MiniBooNE Collaboration), *Updated MiniBooNE neutrino oscillation results with increased data and new background studies*, Physical Review D,

vol. **103**, no. 5, (2021) [arXiv:2006.16883]

[3] C. Athanassopoulos, *et al.* (LSND Collaboration), *Evidence for $\overline{\nu}_\mu \to \overline{\nu}_e$ Oscillations from the LSND Experiment at the Los Alamos Meson Physics Facility*, Physical Review Letters, vol. **77**, no. 15, (1996) 3082-3085

[4] R. Acciarri, *et al.* (MicroBooNE Collaboration), *Design and Construction of the MicroBooNE Detector*, Journal of Instrumentation, vol. **12**, no. 02, (2017) P02017 [arXiv:1612.05824]

[5] P. Abratenko, *et al.* MicroBooNE Collaboration, *Search for an anomalous excess of charged-current quasi-elastic ν_e interactions with the MicroBooNE experiment using Deep-Learning-based reconstruction*, (2021) [arXiv:2110.14080]

[6] P. Abratenko, *et al.* (MicroBooNE Collaboration), *Vertex-Finding and Reconstruction of Contained Two-track Neutrino Events in the MicroBooNE Detector*, Journal of Instrumentation, vol. **16**, no. 02, (2021) P02017 [arXiv:2002.09375]

[7] D. Cianci, *A Deep-Learning-Based Muon Neutrino CCQE Selection for Searches Beyond the Standard Model with MicroBooNE*, Ph.D dissertation, Columbia U., (2021)

[8] P. Abratenko, *et al.* (MicroBooNE Collaboration), *New CC0π GENIE Model Tune for MicroBooNE*, Physical Review D, vol. **105**, no. 7, (2022) 072001 [arXiv:2110.14028]

[9] A. A. Aguilar-Arevalo, *et al.* (MiniBooNE Collaboration), *A Search for muon neutrino and antineutrino disappearance in MiniBooNE*, Physical Review Letters, vol. **103**, no. 6, (2009) 061802 [arXiv:0903.2465]